Journal for ImmunoTherapy of Cancer

CircITGB6 promotes ovarian cancer cisplatin resistance by resetting tumor-associated macrophage polarization toward the M2 phenotype

Han Li,[1,2,3] Fan Luo,[1] Xingyu Jiang,[1] Weijing Zhang,[1] Tong Xiang,[1,3] Qiuzhong Pan,[1,3] Liming Cai,[4] Jingjing Zhao,[1,3] Desheng Weng,[1,3] Yue Li,[1] Yuhu Dai,[5] Fengze Sun,[1,3] Chaopin Yang,[1,3] Yue Huang,[1,3] Jieying Yang,[1,3] Yan Tang,[1,3] Yulong Han,[1,3] Mian He,[6] Yanna Zhang,[1] Libing Song,[1] Jian-Chuan Xia [1,3]

To cite: Li H, Luo F, Jiang X, *et al*. CircITGB6 promotes ovarian cancer cisplatin resistance by resetting tumor-associated macrophage polarization toward the M2 phenotype. *Journal for ImmunoTherapy of Cancer* 2022;**10**:e004029. doi:10.1136/jitc-2021-004029

► Additional supplemental material is published online only. To view, please visit the journal online (http://dx.doi.org/10.1136/jitc-2021-004029).

HL, FL, XJ and WZ contributed equally.

Accepted 06 February 2022

For numbered affiliations see end of article.

Correspondence to
Professor Jian-Chuan Xia; xiajch@mail.sysu.edu.cn

Libing Song; songlb@sysucc.org.cn

Professor Yanna Zhang; zhangyn@sysucc.org.cn

ABSTRACT

Background Platinum resistance is a major challenge in the clinical treatment of advanced ovarian cancer (OC). Accumulating evidence shows that the tumor-promotive M2 macrophage is linked to the limiting chemotherapy efficacy of multiple malignancies including OC. Circular RNAs (circRNAs) are a novel class of non-coding RNAs which function as the critical regulator in biological process of cancer. However, their impact on macrophage polarization and chemoresistance of OC remain unclear.

Methods Platinum-resistant circRNAs were screened using circRNA deep sequencing and validated using in situ hybridization in OC tissues with or without platinum resistance. The role of circITGB6 in inducing cisplatin (CDDP) resistance was evaluated by clone formation, immunofluorescence and annexin V assays in vitro, and by intraperitoneal tumor model in vivo. The mechanism underlying circITGB6-mediated tumor-associated macrophage (TAM) polarization into M2 phenotype was investigated using RNA pull-down, luciferase reporter, electrophoretic mobility shift, RNA binding protein immunoprecipitation (RIP), ELISA and immunofluorescence assays.

Results We identified that a novel circRNA, circITGB6, robustly elevated in tumor tissues and serums from patients with OC with platinum resistance, was correlated with poor prognosis. circITGB6 overexpression promoted an M2 macrophage-dependent CDDP resistance in both vivo and vitro. Mechanistic research determined that circITGB6 directly interacted with IGF2BP2 and FGF9 mRNA to form a circITGB6/IGF2BP2/FGF9 RNA–protein ternary complex in the cytoplasm, thereby stabilizing FGF9 mRNA and inducing polarization of TAMs toward M2 phenotype. Importantly, blocking M2 macrophage polarization with an antisense oligonucleotide targeting circITGB6 markedly reversed the circITGB6-induced CDDP resistance of OC in vivo.

Conclusions This study reveals a novel mechanism for platinum resistance in OC and demonstrates that circITGB6 may serve as a potential prognostic marker and a therapeutic target for patients with OC.

INTRODUCTION

Ovarian cancer (OC) has been reported to be the most lethal cancer among gynecological malignancies with a 5-year survival rate of less than 30%.[1 2] Front-line treatment of OC consists of cytoreductive surgery and a combination of platinum-based chemotherapy.[3] These treatments yield a high initial response rate, usually inducing clinical remission. However, approximately 70% of OC cases will relapse, and the tumors eventually become strongly refractory to platinum-containing chemotherapy.[4] Poor understanding of the underlying mechanisms of OC platinum resistance and tumor relapse poses a major challenge for OC treatment. Therefore, exploration of the molecular contributors of cisplatin (CDDP) resistance and development of new targeted treatments for OC are urgently needed.

Emerging research has shown that cancer cells interact extensively with the tumor microenvironment (TME) to maintain tumor proliferation, metastasis, and drug resistance.[5] The TME of OC is highly immunosuppressive and consists of tumor-associated macrophages (TAMs), myeloid-derived suppressor cells (MDSCs), regulatory T cells (Tregs), dendritic cells (DCs), and neutrophils.[6 7] Previous studies have shown that TME was recognized to be necessary for the maintenance of chemoresistance in OC.[8 9] Macrophages are the preponderant infiltrating immune cells in the TME of OC tissue, which has high plasticity and can be divided into two functional forms depending on the local TME: classically activated macrophages (M1 macrophages, proinflammatory with antitumor activity) and alternatively activated

macrophages (M2 macrophages, anti-inflammatory with protumor progression activity).[10 11] An elevated proportion of M2 macrophages in the TME of OC such as that observed with malignancy-associated ascites) is strongly associated with tumor growth, invasion, immune evasion, and chemoresistance.[12 13] Despite these reports on TAMs, limited research data are available regarding the precise roles of TAMs in processes related to OC progression, especially chemoresistance. Moreover, how TAMs are educated on their phenotype and function by TME and the molecular mechanisms of the related changes remain unclear. Therefore, strategies aiming to target critical molecules regulating OC cell–TAM interaction and chemoresistance may provide novel therapeutic targets to prevent and combat chemoresistance.

Circular RNAs (circRNAs) present a class of single-stranded non-coding RNAs with a covalently closed structure lacking 5′ and 3′ ends and a poly(A) tail.[14] circRNAs have unique advantages as non-invasive and stable biomarkers for human disease diagnosis and prognosis because they are unaffected by RNase R, deadenylation, or cap removal.[15] In recent years, numerous studies have shown that dysregulated expression of circRNAs is associated with the pathogeneses of distinct human disorders, such as cardiovascular disorders, diabetes, and cancer.[16–18] In particular, circRNAs play pivotal roles in cancer proliferation, metastasis, and chemoresistance through different functional mechanisms, including miRNA sponges, RNA-binding protein (RBP) interactions, gene transcription and translation regulators, and encoding functional peptides.[19 20] Moreover, a large number of studies have demonstrated that circRNAs regulate various aspects of the TME.[21] However, the identities of pivotal circRNAs and their functions, as well as the underlying mechanisms of the crosstalk between OC cells and TME (especially TAMs)-mediated OC chemoresistance, are still largely enigmatic.

In the present study, we performed next-generation sequencing (NGS) and screened a specific circRNA, hsa_circ_0056856 (termed circITGB6), that is involved in OC chemoresistance and associated with unfavorable prognosis. Further investigations reveal that circITGB6 enhances the stability of *FGF9* mRNA through interaction with IGF2BP2, which subsequently shifts macrophages toward M2 phenotype in the TME and consequently induces CDDP resistance in OC cells. Clinically, elevated circITGB6 and FGF9 are more prevalent in CDDP-resistant OC tissues than in CDDP-sensitive OC tissues. Collectively, our studies show that the interaction between TAMs and cancer cells is a key mechanism of chemoresistance in patients with OC. These findings suggest that upregulation of circITGB6 correlates with the poor response of CDDP in OC.

MATERIALS AND METHODS

The complete experimental protocols are described in the online supplemental material.

RESULTS

Elevated levels of circITGB6 correlate with chemoresistance and poor prognosis in OC

CircRNA-seq revealed a total of 30 circRNAs that were remarkably altered with $\log_2^{\text{fold change (FC)}}$ values of >2 or $\log_2^{\text{FC}}$ of <−2, and a p value of <0.05 in chemoresistant OC tissues compared with chemosensitive OC tissues (figure 1A). In order to further identify the circRNAs correlated with CDDP resistance, we performed quantitative real-time PCR (qRT-PCR) to measure the expression levels of the top 10 upregulated circRNAs in 40OC tissues. The tumors from chemoresistant patients with OC displayed remarkably higher expression of circITGB6 but not of the other nine circRNAs than those from patients who did not exhibit postoperative CDDP resistance (figure 1B). We then examined the expression of circITGB6 in human OC cell lines and found that it was remarkably higher in all six human OC cell lines than in the non-neoplastic cell line HosePic (online supplemental figure 1A). We also detected the levels of circITGB6 in OC tissues and normal ovarian epithelial tissues, and the results showed that circITGB6 levels in OC tissues were significantly higher than those in normal tissues (online supplemental figure 1B). Notably, circITGB6 expression levels were remarkably upregulated in serum obtained from patients with OC with CDDP resistance compared with serum obtained from CDDP-sensitive patients with OC and normal controls (figure 1C). Moreover, OC patients with CDDP significantly upregulated tumor circITGB6 levels had relatively low overall survival and a higher relapse rate than patients with low tumor circITGB6 expression. Therefore, high expression of circITGB6 may be a prognostic factor (figure 1D,E, and online supplemental figure 1). Subsequently, we characterized the structure of circITGB6 and found that it is formed by back-splicing of exons 10 and 11 of integrin subunit beta 6 (*ITGB6*) (figure 1F). As shown in figure 1G, the circITGB6 amplification product was detected only in cDNA by divergent primers; no products were amplified from genomic DNA (gDNA) (figure 1G). High stability is a key feature of circRNAs.[20] Thus, to verify the stability of the circRNA, RNase R exonuclease was used to pretreat the RNAs. The results indicate that the circular form of *ITGB6* was resistant to RNase R, while the linear *ITGB6* RNA was remarkably degraded after RNase R treatment (figure 1H and online supplemental figure 1D,E). Moreover, the half-life of circITGB6 was significantly longer than that of linear ITGB6 mRNA (figure 1I,J). Then, we performed nuclear and cytoplasmic RNA extraction and FISH to detect that circITGB6 was localized mainly in the cytoplasm of OC cells (figure 1K, L).

Chemoresistance of OC in vivo induced by circITGB6 is TME-dependent

Given the significant clinical relevance of circITGB6 in OC CDDP resistance, we explored the in vivo functional role of circITGB6 in this process. CircITGB6 was successfully upregulated by transfection with a

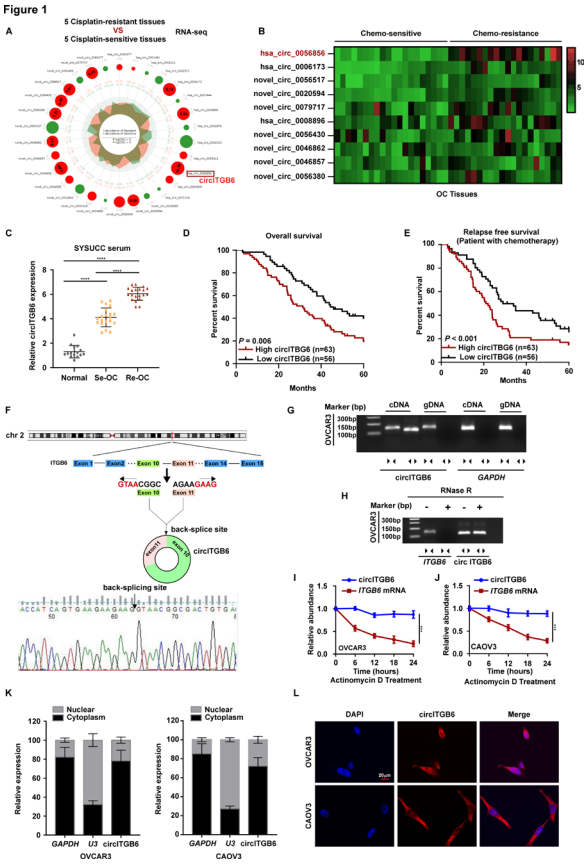

Figure 1 Elevated levels of circITGB6 correlates with chemoresistance and poor prognosis in OC. (A) RNA sequencing of five CDDP-resistant and five CDDP-sensitive OC tissues to screen differentially expressed circRNAs. Radar chart showing top 18 upregulated (the red circles) and 12 downregulated (the green circles) circRNAs in CDDP-resistant OC compared with those in CDDP-sensitive OC. (B) Heatmap shows top 10 upregulated circRNA expression in 20 CDDP-resistant and 20 CDDP-sensitive OC tissues detected by qRT-PCR. (C) qRT-PCR analysis of circITGB6 expression in serum from 15 normal control, 20 patients with OC with CDDP resistance and 20 patients with OC with CDDP sensitivity from the SYSUCC. Data represent mean±SD. The p values were determined by unpaired Student's t-test. (D,E) Kaplan-Meier analysis of OS and RFS in patients with OC with low expression versus high expression in the circITGB6 from SYSUCC cohorts. The p value was determined by a log-rank test. (F) Schematic illustration showed the circularization of *ITGB6* exons 10 and 11 to form circITGB6. The back-splicing junction of circITGB6 was verified by RT-PCR and Sanger sequencing. (G) circITGB6 expression in OVCAR3 cells verified by RT-PCR. Agarose gel electrophoresis showed that divergent primers amplified circITGB6 in cDNA but not gDNA. GAPDH served as a negative control. (H) Validation of circITGB6 stability by RNase R treatment and RT-PCR analysis. Data represent mean±SD from three independent experiments; The p value was determined by two-tailed unpaired Student's t-test. (I,J) qPCR analysis of the abundance of circITGB6 and linear *ITGB6* in OVCAR3 and CAOV3 cells treated with actinomycin D at the indicated times. Data represent mean±SD from five independent experiments; dot plot reflects data points from independent experiment. The p value was determined by two-way analysis of variance. (K) circITGB6 abundance in nuclear and cytoplasmic fractions of OVCAR3 and CAOV3 cells was evaluated by qRT-PCR. GAPDH acted as a positive control in the cytoplasm, and U3 acted as a positive control in the nucleus. Data represent mean±SD from three independent experiments; (L) localization of circITGB6 in OVCAR3 and CAOV3 cells was detected by FISH. Nuclei were stained with DAPI (blue) and circITGB6 probes were labeled with Cy3 (red). Results are presented as means±SD.D. of a representative experiment performed in triplicate. ***P<0.001, ****P<0.0001. CDDP, cisplatin; circRNA, circular RNA; DAPI, 4',6-diamidino-2-phenylindole; GAPDH, glyceraldehyde-3-phosphate dehydrogenase; DNA, genomic DNA; ns, no significance; OC, ovarian cancer; OS, overall survival; qRT-PCR, quantitative real-time PCR; RFS, relapse-free survival; RT-PCR, quantitative real-time PCR.

circITGB6-overexpressing plasmid and downregulated by transfection with sh-circITGB6, targeting the back-splicing region of circITGB6. In addition, the results showed that overexpression and knockdown of circITGB6 had no impact on the expression of the host gene *ITGB6* (online supplemental figure 1F-L). To assess the functions of circITGB6 in OC, luciferase-labeled ID8 cells with overexpression or knockdown of circITGB6 were intraperitoneally injected into female C57BL/6 mice. The mice in the circITGB6-overexpressing group showed a much stronger luciferase signal and more hemorrhagic ascites after CDDP treatment than the mice in the control group; in contrast, we detected markedly lower luciferase activity and less hemorrhagic ascites in the sh-circITGB6 group than in the control group (figure 2A–C). Moreover, the survival times of the circITGB6-overexpressing group of mice were shorter than those of the vector-control mice, and the survival times of the mice bearing

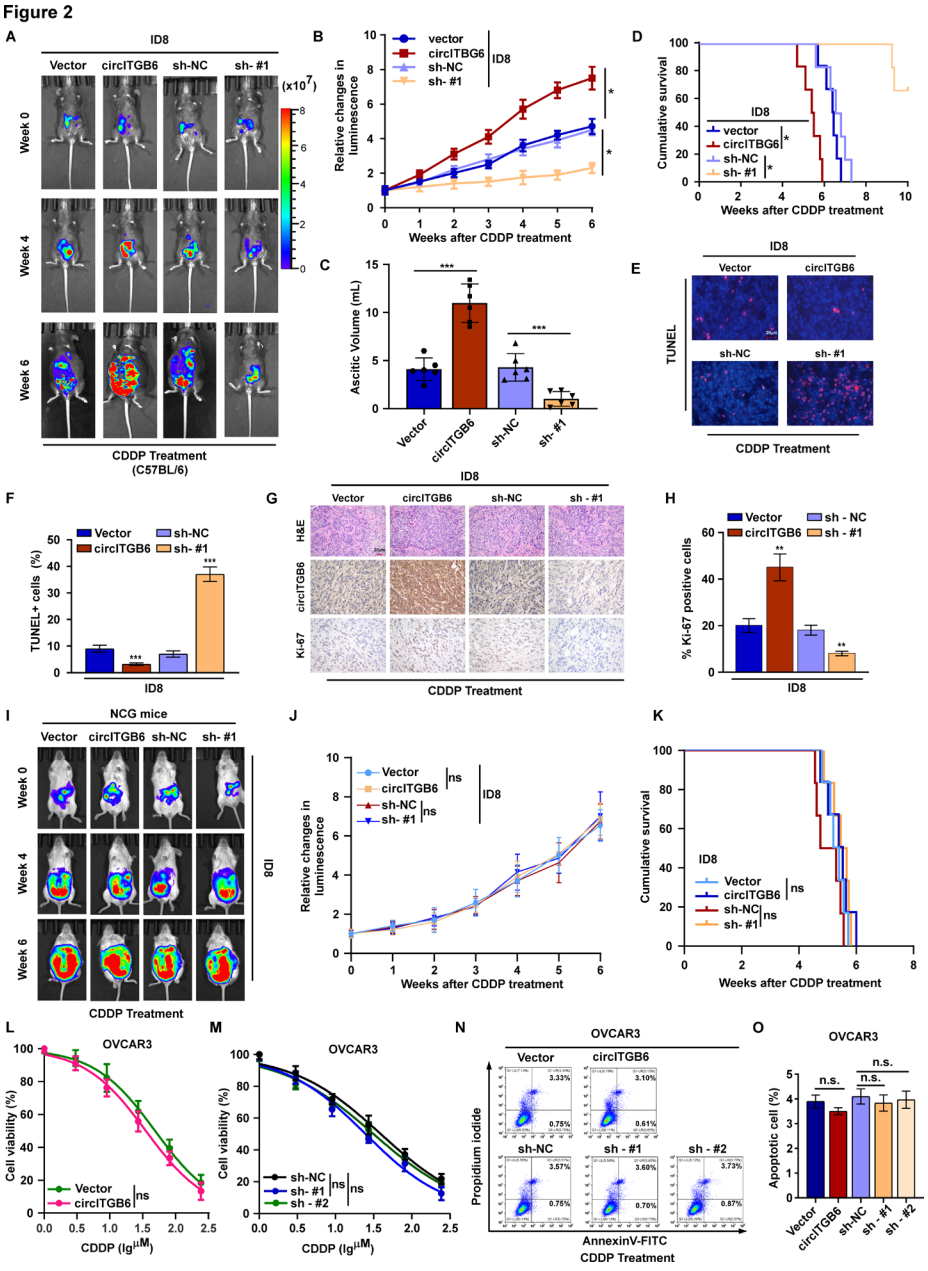

Figure 2 Chemoresistance of OC in vivo induced by circITGB6 is TME-dependent. Representative images of CDDP-treated intraperitoneal tumor-bearing C57BL/6 mice in each group at the indicated time. (B) Relative changes in bioluminescence signal of intraperitoneal tumors in C57BL/6 mice in each group on CDDP chemotherapy. (C) Kaplan-Meier survival of CDDP-treated intraperitoneal tumor-bearing C57BL/6 mice. (D) The tumor ascites volume of CDDP-treated intraperitoneal tumor-bearing C57BL/6 mice from each group was measured. (E,F) TUNEL-stained cells in indicated tumors. The proportion of TUNEL-positive cells was qualified from five random fields, representing the apoptotic index. (G) ISH assay of circITGB6 and IHC staining of Ki67, and H&E analysis and (H) quantification of proliferation index in the indicated xenograft tumors. (I) Representative images of CDDP-treated intraperitoneal NCG mice in each group at the indicated time. (J) Relative changes in bioluminescence signal of intraperitoneal tumors in NCG mice in each group on CDDP chemotherapy. (K) Kaplan-Meier survival of CDDP-treated intraperitoneal tumor-bearing NCG mice. (L,M) MTT cell viability assay in the indicated cells. (N,O) FACS analysis of annexin V/PI staining and quantification of indicated cells treated with CDDP (5 μM) after 24 hours. Results are presented as means±SD of a representative experiment performed in triplicate. *P<0.05, **P<0.01, ***P<0.001. CDDP, cisplatin; MTT, 3-(4,5)-dimethylthiahiazo (-z-y1)-3,5-di- phenytetrazoliumromide; ns, no significance; OC, ovarian cancer; TME, tumor microenvironment; V/PI, annexin V/propidium iodide.

circITGB6-silenced cells were longer than those of the control mice under CDDP treatment (figure 2D). Immunohistochemistry (IHC) of tumor xenografts showed that the number of KI-67^{+} cancer cells was notably increased and that the number of TUNEL^{+} (TdT mediated dUTP Nick End Labeling) cells was remarkably decreased on circITGB6 upregulation (assessed by in situ hybridization (ISH)) under CDDP treatment (figure 2E–H). Moreover,

overexpressing or silencing circITGB6 induced no statistically significant change in the colony formation capacity of OC cells in the absence of CDDP treatment (online supplemental figure 2A-C).

However, whether circITGB6 mobilized other tumor-fighting mechanisms by interacting with the host immune system for its antitumor effects was still unclear. Intriguingly, in severely immunodeficient NCG mice, we found that the antitumor effect of CDDP against ID8 OC cells was lost (figure 2I–K). Additionally, we conducted a series of in vitro studies and found that compared with control cells, neither circITGB6-overexpressing nor circITGB6-knockdown cells showed significant alterations in the half-maximal inhibitory concentration (IC_{50}) of CDDP or in colony-forming ability under CDDP treatment in monoculture (figure 2L,M, and online supplemental figure 3A-E). Moreover, we found that CDDP-induced apoptotic death was not obviously reduced or increased in circITGB6-overexpressing or circITGB6-silenced cells compared with the control cells in monoculture (figure 2N,O, and online supplemental figure 3F-J). In addition, we also found that circITGB6 has no significant impact on the proliferation and CDDP resistance of ID8 cells in vitro (online supplemental figure 4A,B).

circITGB6 induces macrophage polarization toward an M2 phenotype

As this finding was inconsistent with circITGB6-induced CDDP resistance in C57BL/6 mice, we further explored whether other key factors confer CDDP resistance in OC. Recent advances in cancer immunology have demonstrated that the therapeutic resistance of cancers also depends considerably on extrinsic mechanisms mediated by the crosstalk between cancer cells and other infiltrated cellular components of the TME, particularly immune cells.[22]

To explore the possibility that circITGB6 expression regulates cancer cell interactions with infiltrating immune cells in tumor tissues, we conducted a cell enrichment analysis (xCell) based on the bulk RNA-seq.[23] Intriguingly, among the different kinds of infiltrating immune cells, macrophages were strongly and remarkably positively correlated with circITGB6 expression (figure 3A). Moreover, recent studies have reported that TAMs constitute the preponderant infiltrating immune cell population in the OC TME, where they are reported to not only promote tumor angiogenesis and metastasis but also induce chemotherapy resistance and suppress the antitumor immune response.[24] Macrophages with the M2 phenotype are intrinsically capable of exerting tumor-promoting effects. To determine whether macrophages are involved in CDDP-mediated antitumor effects, we treated mice with clodronate liposomes (online supplemental figure 5A). We found that macrophage depletion disrupted the antitumor effect of CDDP on ID8 OC growth (figure 3B and online supplemental figure 5B). In addition, we further verified the macrophage-dependent CDDP resistance in circITGB6-overexpressed ID8 cells, which indicated that macrophage depletion significantly abolished the circITGB6-mediated suppressive effects (online supplemental figure 5C). Moreover, analysis of the data from The Cancer Genome Atlas (TCGA) via CIBERSORT algorithm showed that TAMs indeed constituted the preponderant infiltrating immune cell population in the TME of OC (online supplemental figure 6A,B). Additionally, the potential role of circITGB6 in other stromal cells, including $CD8^+$ T cells and Treg cells was further determined. Notably, the circITGB6 expression was almost undetectable examined by qRT-PCR and FISH assays in the aboved-mentioned stromal cells of OC (online supplemental figure 7A-D). These findings indicated that circITGB6 was originated from the OC cells instead of the stromal immune cells. Importantly, M2-type macrophages were significantly increased in patients with platinum-resistant compared with platinum-sensitive patients with OC, but there was no difference between M1-type and M0-type macrophages in TCGA data (figure 3C–E). We further assessed the clinical significance of circITGB6 expression in 119 paraffin-embedded OC specimens (online supplemental table S1). Consistently, ISH revealed that circITGB6 was significantly upregulated in CDDP-resistant OC specimens compared with CDDP-sensitive specimens (figure 3F,G, and online supplemental figure 1). Notably, CD206 staining showed that the number of infiltrated M2 macrophages ($CD206^+$ macrophages) was robustly increased in OC tissues with high circITGB6 expression (figure 3F–H). Moreover, correlation analysis indicated that the CDDP response status and high circITGB6 expression were positively associated with $CD206^+$ macrophage infiltration in OC (figure 3I,J, and online supplemental table 1). Therefore, these results suggest that circITGB6 upregulation might contribute to CDDP resistance in OC through resetting TAM polarization toward the M2 phenotype.

Next, we investigated whether monocytes could be differentiated into M2-type macrophages via incubation with conditioned medium (CM) from OVCAR3 cells stably transfected with circITGB6, sh-circITGB6#1, or CM from control cells (figure 3K). Fluorescence activating cell sorter analysis (FACS) showed that the percentage of $CD206^+$ macrophages was higher in the interleukin (IL)-4-treated group than in the untreated group, while $HLA\text{-}DR^+$ macrophages were mainly induced after interferon gamma (IFN-γ) and lipopolysaccharide (LPS) treatment (figure 3L,M). Treatment of macrophages with CM from circITGB6-overexpressing OVCAR3 cells induced more $CD206^+$ macrophages and fewer $HLA\text{-}DR^+$ macrophages than CM derived from the control group (figure 3N,O).

Furthermore, we collected serum from patients with OC, including six patients with OC with high circITGB6 expression and six patients with OC with low circITGB6 expression in their OC tissues assessed by ISH. Notably, circITGB6 levels were significantly upregulated in serum deprived from patients with OC with high circITGB6 expression compared with patients with OC with low circITGB6 expression (online supplemental figure

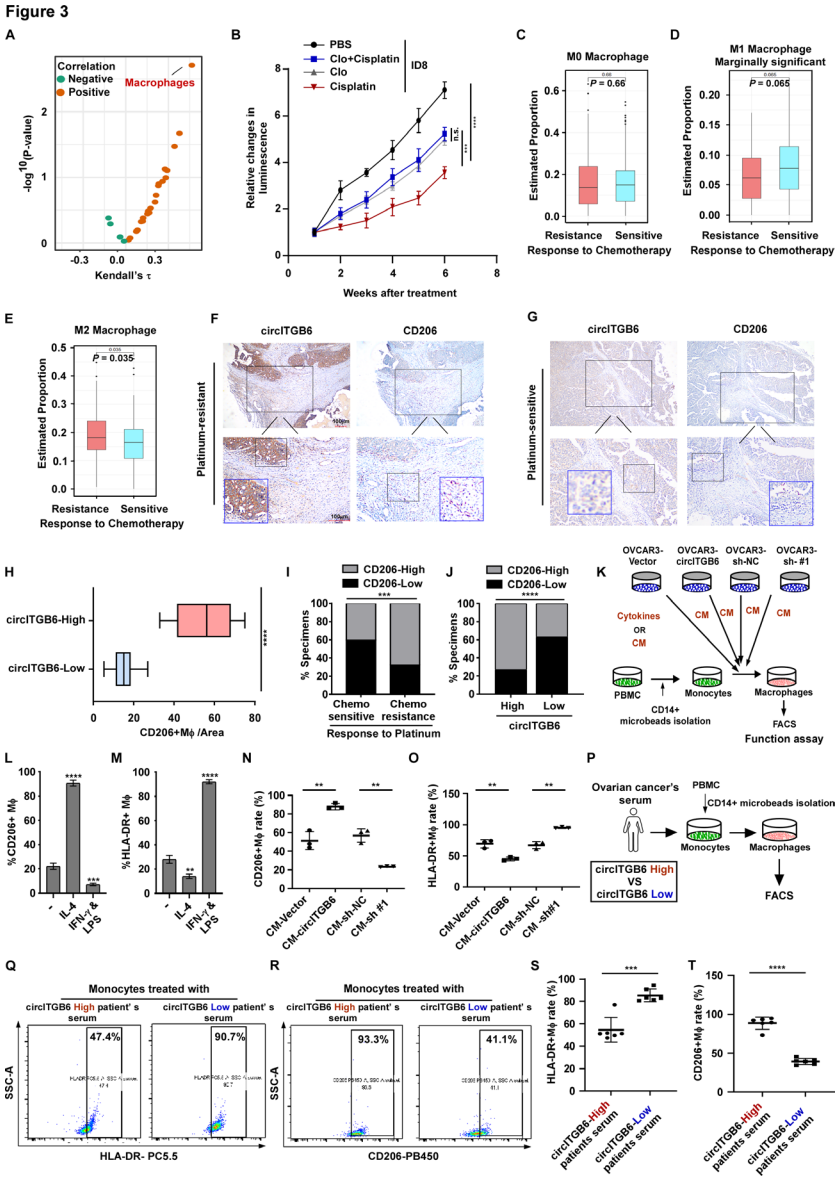

Figure 3 CircITGB6 induces macrophage polarization toward an M2 phenotype. (A) The scatter plot depicts Kendall's τ correlation coefficient between circITGB6 abundance and cell-enrichment scores versus the associated cell-enrichment p value significance. (B) C57BL/6 mice (n=6) intraperitoneal bearing ID8 cells with or without clodronate liposome treatment were injected with PBS or cisplatin for 6 weeks (Clo). The tumor growth was followed. (C–E) Different subtypes of macrophage-infiltrated proportion in the TEM of OC analyzed from TCGA via CIBRSORT software. (F,G) Representative image of circITGB6 and CD206 of chemoresistant and chemosensitive OC specimens. (H) Quantification of $CD206^+$ macrophages in circITGB6-low or circITGB6-high specimens. (I,J) Correlation analyses between $CD206^+$ macrophage-infiltrated status and chemotherapy response status or circITGB6 expression in OC patient specimen. (K–M) Schematic: (K) in vitro-polarized macrophages. (L,M) % $CD206^+$ or %HLA-DR+ macrophages after treatment with IL-4 or IFN-γ and LPS or media only (–). (N,O) FACS dot plots showing % $CD206^+$ and %HLA-DR+ macrophages after treatment with CM collected from indicated cells. (P) Schematic shows TAM polarization in vitro with serum from patients with OC with circITGB6 high or circITGB6 low and (Q–T) representative FACS dot plots from patients showing % $CD206^+$ and %HLA-DR+ macrophages after treatment (with circITGB6 high or circITGB6 low serum) of patient with OC. Results are presented as means±SD of a representative experiment performed in triplicate. **P<0.01, ***P<0.001, ****P<0.0001. Clo, clodronate liposome; CM, conditioned medium; IFN-γ, interferon gamma; IL, interleukin; ns, no significance; OC, ovarian cancer; TAM, tumor-associated macrophage; TCGA, The Cancer Genome Atlas; TEM, tumor microenvironment.

9A). We treated peripheral blood mononuclear cell (PBMC) -derived monocytes obtained from healthy female donors with the serum (figure 3P). Compared with low circITGB6- OC patient-derived serum, high circITGB6-OC patient-derived serum induced a higher percentage of $CD206^+$ macrophages and lower $HLA\text{-}DR^+$ macrophages (figure 3Q–T). Therefore, factors in serum derived from patients with high or low circITGB6 expression induce macrophage polarization comparable to that

induced by CM collected from OC cells with high or low circITGB6 expression.

Next, we further explored the effect of tumor-derived circITGB6 on M2 macrophage polarization in vivo and found that a higher level of circITGB6 in tumor tissues was accompanied by higher infiltration of F4/80^{+}CD206^{+} TAMs (M2) and lower infiltration of F4/80^{+}CD80^{+} TAMs (M1) (figure 4O,P, and online supplemental

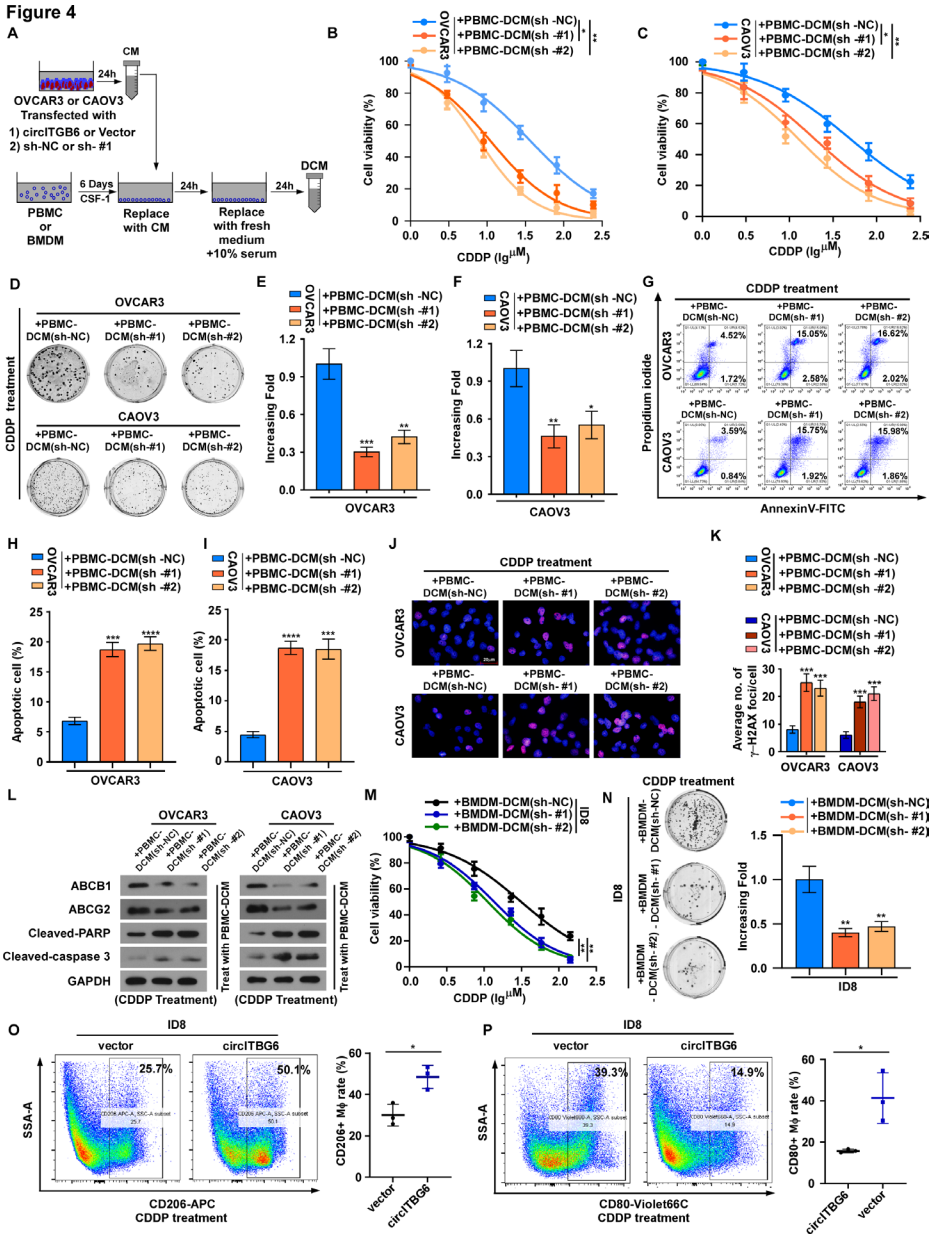

Figure 4 Essential role of TAMs (M2 phenotype) in circITGB6-regulated OC CDDP resistance. (A) Scheme of the workflow: OVCAR3 and CAOV3 cells were stably transiently with circITGB6 or sh-circITGB6#1 or its corresponding control (*vector* or *sh-NC*), and according to the flowchart to collected DCM for subsequent functional experiments. (B,C) MTT cell viability assay in the OC cells with the indicated PBMC-derived DCM treatment. (D–F) Representative images (D) and quantification (E,F) of colony number of the OC cells with the indicated DCM treatment. (G–I) FACS analysis of annexin V/PI staining (G) and quantification (H,I) of the OC cells with the OC cells PBMC-derived DCM and CDDP (5 μM) treatment. (J,K) Representative images and quantification of γ-H2AX in the OC cells with the indicated PBMC- derived DCM and CDDP (5 μM) treatment. (L) Immunoblot analysis of expression levels of indicated protein in the OC cells with the indicated PBMC-derived DCM and CDDP (5 μM) treatment. GAPDH served as the loading control. (M) MTT cell viability assay in the OC cells with the indicated BMDM-derived DCM treatment. (N) Representative images (left) and quantification (right) of colony number of the indicated cells with its corresponding BMDM-derived DCM treatment. (O,P) Proportion of CD206^{+} macrophages and CD80+ macrophages isolated from intraperitoneal tumor-bearing C57BL/6 mice injected with indicated cells was measured by FACS analysis. Results are presented as means±SD of a representative experiment performed in triplicate. *P<0.05, **P<0.01, ***P<0.001, ****P<0.0001. BMDM, bone marrow-derived macrophage; CDDP, cisplatin; CM, conditioned medium; DCM, double-conditioned medium; ns, no significance; TAM, tumor-associated macrophage.

figure 10A-C). In addition, overexpression of circITGB6 enhanced the expression of the M2 marker IL-10 and decreased the M1 marker IL-6 in serum collected from the mice (as examined by ELISA), whereas circITGB6 knockdown had the opposite effect (online supplemental figure 10D, E). Moreover, TAMs isolated from circITGB6-overexpressing ID8 tumors produced less tumor necrosis factor -alpha (TNF-α), inducible nitric oxide synthase (iNOS) and IL-6 and more Arg1 and IL-10 than TAMs collected from control ID8 tumors, as examined by qRT-PCR (online supplemental figure 10F–J).

Essential role of TAMs (M2 phenotype) in circITGB6-regulated OC CDDP resistance

To evaluate how the presence of M2-type macrophages functionally educates OC cells to induce chemoresistance, we treated cells with double-conditioned medium (DCM)[25] (figure 4A). Primary human PBMC-derived $CD14^+$ monocytes were isolated from healthy donors for further exploration. Primary human macrophages were first stimulated with CM derived from OC cells stably transfected with circITGB6-vector, sh-circITGB6#1, or sh-circITGB6#2 for 24 hours before incubation in fresh medium for 24 hours (DCM). This DCM was then used to treat parental OC cells with CDDP for further in vitro assays. Compared with that for the control OVCAR3/CAOV3 cells, the IC_{50} value of CDDP was significantly decreased in sh-circITGB6#1 or sh-circITGB6#2 OVCAR3/CAOV3 cell DCM-treated parental OC cells (figure 4B,C). Moreover, in parental OC cells under CDDP administration, incubation in DCM derived from OC cells with circITGB6 silencing resulted in significantly greater CDDP-induced apoptotic death and impaired colony formation than incubation in control cell-derived DCM (figure 4D-I). The formation and persistence of DNA adducts of CDDP are critical for CDDP-induced cancer cell death. Compared with that in cells treated with the DCM obtained from circITGB6 control cells, the number of CDDP-induced γ-H2AX foci was significantly greater in circITGB6-silenced OVCAR3/CAOV3 DCM-treated parental OC cells (figure 4J,K). Additionally, the expression of chemoresistance-related genes, including ABCB1 and ABCG2, was drastically decreased, whereas the expression of cleaved caspase 3 and poly ADP-ribose polymerase (PARP) was drastically increased, in parental OC cells incubated with DCM derived from circITGB6-silenced OC cells (figure 4L). Moreover, we found consistent results in the bone marrow-derived macrophage and OC cell coculture systems (figure 4M,N). In contrast, circITGB6 overexpression had the opposite effect (online supplemental figure 1).

A reduction in drug accumulation in cancer cells has been regarded as a major mechanism promoting CDDP resistance.[26] Interestingly, our CDDP efflux assay revealed that the content of intracellular and gDNA-bound CDDP was greatly elevated in the interior of the OC cells incubated with DCM derived from circITGB6-silenced OC cells (online supplemental figure 12A-B). The results were further validated by an efflux kinetic assay (online supplemental figure 12C, D).

circITGB6 interacts with IGF2BP2 directly

To examine the potential mechanism of circITGB6-induced TAM M2 polarization, we conducted RNA pull-down assays followed by mass spectrometry (MS) analysis with biotinylated circITGB6 and a control probe as a negative control to screen circITGB6-interacting proteins (figure 5A–C and online supplemental table 5). We identified IGF2BP2 as a putative protein that directly binds to circITGB6 and has been reported to be essential for regulating mRNA stability (figure 5A and C). Furthermore, RIP assays confirmed the interaction between circITGB6 and IGF2BP2 (figure 5D). We used immunofluorescence-fluorescence in situ hybridization (IF-FISH) assays to detect the subcellular localization of circITGB6 and IGF2BP2, and the IF-FISH images showed colocalization of circITGB6 and IGF2BP2 in the cytoplasm (figure 5E). These data indicated that circITGB6/IGF2BP2 forms an RNA-protein complex in the cytoplasm. Furthermore, we explored which domain of IGF2BP2 facilitates the interaction with circITGB6. IGF2BP2 mutants with KH domain truncations were used. RIP assays showed that the KH1–two di-domain of IGF2BP2 specifically bound to circITGB6, indicating that the KH1–2 di-domain is essential for interaction with circITGB6 (figure 5F,G). Previous studies have reported that the sequence CAUH (H=A, C or U) is the only consensus recognition motif for IGF2BP2[27] . According to these results, by browsing the exon 10-exon 11 junction sequence in circITGB6, we identified that the CAUC motif located in this sequence was a putative binding motif of IGF2BP2 (figure 5H, top). Furthermore, by performing electrophoretic mobility shift, we confirmed that the CAUC motif inside the junction of circITGB6 is essential for the IGF2BP2 interaction. Super-shift experiments suggested that IGF2BP2 binds to this motif specifically. Formation of the circITGB6/IGF2BP2 complex was remarkably reduced when the CAUC motif was mutated (figure 5H, bottom). These data indicate that IGF2BP2 binds to the CAUC motif of circITGB6 through the KH1–2 di-domain.

circITGB6/IGF2BP2/FGF9 RNA-protein ternary complex stabilizes *FGF9* mRNA

As previous studies have reported that I'GF2BP2 plays a pivotal role in regulating mRNA stability. Thus, we conducted RNA-seq analyses on OVCAR3 cells (*sh-NC* vs *sh-circITGB6*). 86 mRNAs expression showed obviously reduced in *sh-circITGB6* OVCAR3 cells compared with *sh-NC* OVCAR3 cells ($\log_2^{|FC|} > 1.5$). Moreover, we also analyzed the downregulated mRNAs in *sh-NC* OVCAR3 cells versus *sh-circITGB6* OVCAR3 cells that were simultaneously upregulated in chemoresistant OC tissues versus chemosensitive OC tissues (described in figure 1A). Previous studies have also reported that IGF2BP2 preferentially binds to the 3′UTRs of downstream target mRNAs with AU-rich elements. Thus, we screened IGF2BP2-binding 3′UTRs of downstream target mRNAs among the

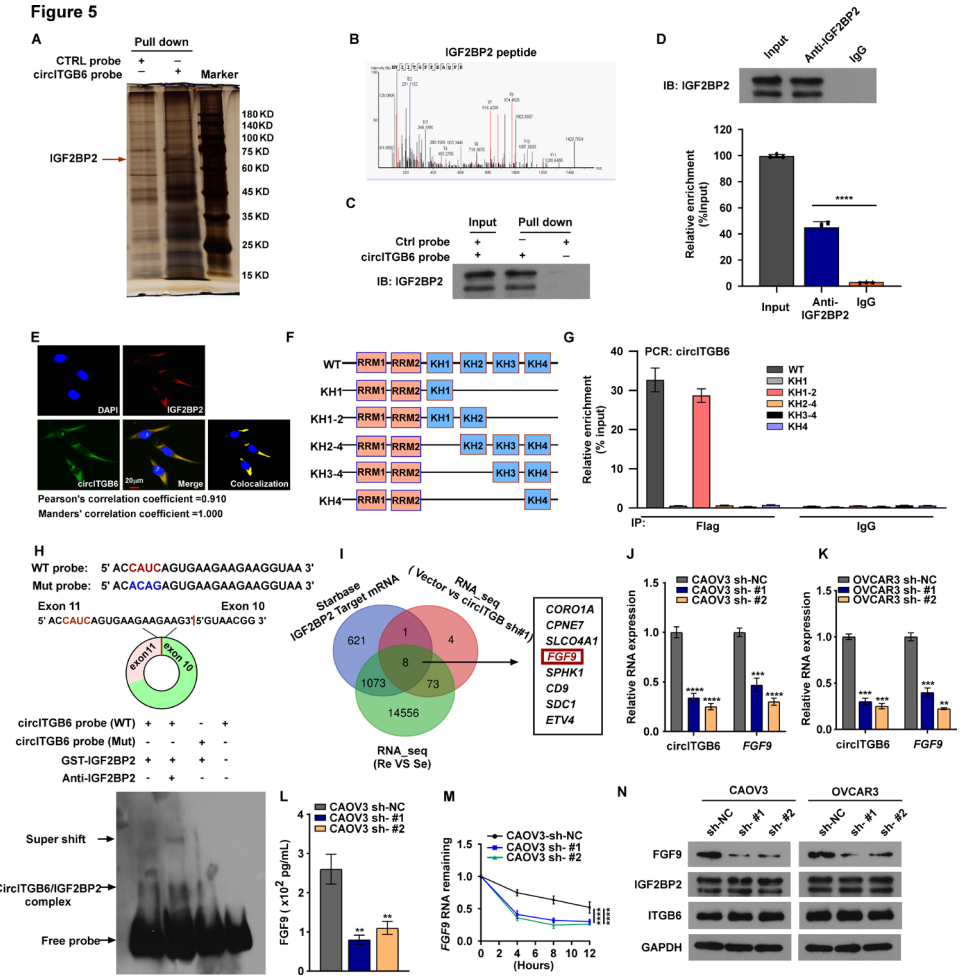

Figure 5 CircITGB6 interacts with IGF2BP2 directly. (A) Identification of the circITGB6–protein complex pulled down by circITGB6 junction probe with protein extracts from OVCAR3 cells. The arrows indicating the additional band presented in the circITGB6–protein complex. (B) MS profiles of target band (corresponding peptide sequences of IGF2BP2 retrieved by circITGB6. (C) Immunoblot analysis of IGF2BP2 after RNA pull-down assay showing its specific association with circITGB6. (D) RIP assays showing the association of IGF2BP2 with circITGB6. Relative enrichment representing RNA levels associated with IGF2BP2 compared with an input control. IgG antibody served as a control. (E) IF-FISH assay showing that circITGB6 is colocalized with IGF2BP2 protein in the cytoplasm. (F) Schematic structures showing RNA-binding domains within IGF2BP2 protein and a summary of IGF2BP2 truncations. (G) Relative enrichment representing circITGB6 levels associated with truncated IGF2BP2 relative to an input control examined by RIP assay. (H) Top: schematic illustration showing the CAUC motif located at exon 10–exon 11 junction site of circITGB6 and the RNA probe for the RNA-EMSA assay; bottom: RNA-EMSA assay showing the binding ability of purified IGF2BP2 with biotin-labeled oligonucleotides containing CAUC motif from circITGB6. (I) The putative mRNA interacting with circITGB6 predicted by StarBase3, RNA_seq (*OVCAR3-vector cells* vs *OVCAR3-circITGB6 sh#1* cells) and RNA_seq (re– vs Se– OC tissues). (J,K) qRT-PCR analysis for the RNA expression of circITGB6 and *FGF9* in control and circITGB6-knockdown OC cells. (L) Expression of *FGF9* in *control and circITGB6-knockdown* OC cells was measured by ELISA. (M) circITGB6 knockdown in OVCAR3 cells significantly downregulated *FGF9* mRNA abundance. (N) Western blotting analysis for the protein expression of FGF9, IGF2BP2, ITGB6 in control and circITGB6-knockdown OC cells. GAPDH was used as an internal control. Results are presented as means±SD of a representative experiment performed in triplicate. *P<0.05, **P<0.01, ***P<0.001, ****P<0.0001. EMSA, electrophoretic mobility shift; ns, no significance; qRT-PCR, quantitative real-time PCR.

upregulated mRNAs mentioned above using published RBP CLIP-seq data sets for different types of cancers in StarBase, an encyclopedia of RNA interactomes.[28] Through the above screening methods, we identified 8 mRNAs bound by IGF2BP2. Considering that circITGB6 induced TAM M2 polarization, only one TAMs M2 polarization-associated secreted factor, *FGF9*, was identified as a potential downstream target of circITGB6 (figure 5I) based on previous research. Furthermore, qRT-PCR assays and ELISA were performed to validate that *FGF9* is the target of circITGB6 (figure 5J–L). We also found that silencing circITGB6 remarkably reduced *FGF9* mRNA stability (figure 5M) and consequently significantly reduced *FGF9* expression (figure 5N).

Using sequence BLAST analysis, we found that two CAAAC sites inside circITGB6 could directly bind to the 3′UTR of *FGF9* (GUUUG motif) rich in AU elements (figure 6A). Next, we used a series of in vitro assays to investigate the interaction of circITGB6 and *FGF9* mRNA to confirm the interaction

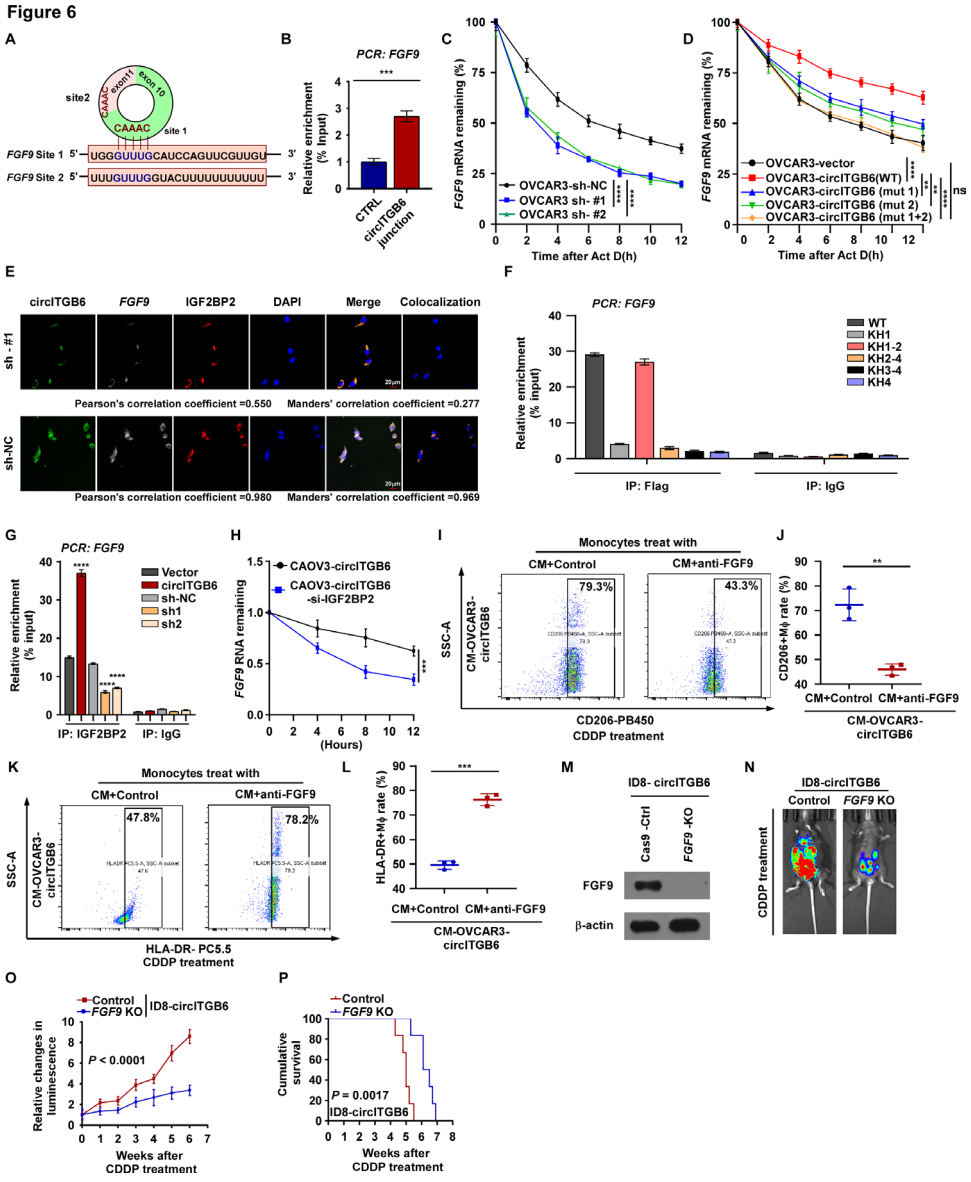

Figure 6 The circITGB6/IGF2BP2/FGF9 RNA-protein ternary complex stabilizes FGF9 mRNA. (A)Top: sequence blast analysis showing that circITGB6 directly targets the 3′UTR of *FGF9* with high Au content. (B) Relative enrichment representing and *FGF9* RNA levels associated with circITGB6 junction compared with control. (C,D) RNA was isolated at the indicated time points and then subjected to qRT-PCR analysis of FGF9 in the indicated OVCAR3 cell treated with ActD (5 µg/mL). (E) IF-FISH assay indicated that the colocalization of circITGB6/IGF2BP2/*FGF9* was decreased on knockdown of circITGB6. (F) Relative enrichment representing the enrichment of *FGF9* associated with truncated IGF2BP2 protein complex compared with an input control. IgG antibody served as a control. (G) RIP assays showing the association of IGF2BP2 with *FGF9* on circITGB6 silencing or overexpression. The p values were determined by a two-tailed unpaired Student t-test. (H) IGF2BP2 knockdown in *CAOV3-circITGB6* overexpression cells remarkably reduced *FGF9* mRNA abundance. (I–L) FACS dot plots showing (I) % $CD206^+$ and (L) %HLA-DR+ macrophages after treatment with CM collected from indicated cells with anti-FGF9 neutralizing antibody or not. (M) Western blot showing expression of FGF9 in ID8 cells with CRISPR/Cas9-mediated knockout of *FGF9* (*FGF9*–KO). (N) Representative images of indicated groups of mice with administration of CDDP chemotherapy. (O,P) Relative changes in bioluminescence signal and Kaplan-Meier survival of indicated groups of mice with administration of CDDP. Results are presented as means±SD of a representative experiment performed in triplicate. **P<0.01, ***P<0.001, ****P<0.0001. CM, conditioned medium; CDDP, CDDP, cisplatin; ns, no significance.

via circRNA pull-down assays (figure 6B and online supplemental figure 13A). Next, we explored whether the circITGB6/*FGF9* mRNA complex is essential for maintenance of *FGF9* mRNA stability. Moreover, the half-life of *FGF9* mRNA was shortened in circITGB6- silencing cells but prolonged in circITGB6-overexpressing cells (WT) (figure 6C,D). Furthermore, the half-life of FGF9 mRNA was significantly shortened in circITGB6-overexpressing cells when the binding site 1 or 2 in circITGB6 was mutated compared with that in circITGB6-overexpressing cells (WT). However, when the binding sites 1 and 2 in circITGB6 were mutated, there was no statistical difference in the half-life of FGF9 mRNA between

circITGB6-overexpressing cells (Mut1+2) and control cells (figure 6D). The colocalization of the IGF2BP2/*FGF9* RNA–protein complex was significantly reduced when circITGB6 was knocked down, while IGF2BP2 expression was unchanged (figure 6E). RIP assays demonstrated that the KH1–2 di-domain of IGF2BP2 was essential for its interactions with circITGB6 and *FGF9* (figures 5G and 6F). Additionally, silencing circITGB6 significantly decreased the *FGF9*/IGF2BP2 RNA–protein interaction, as detected by RIP assays, whereas upregulation of circITGB6 remarkably increased the enrichment of *FGF9* in IGF2BP2-immunoprecipitated fractions (figure 6G and online supplemental figure 13B-D). Additionally, we further observed that the mRNA stability of *FGF9* was remarkably reduced on knockdown of IGF2BP2 (figure 6H). These data show that circITGB6 plays a critical role in promoting the interactions between IGF2BP2 and *FGF9* and increases the mRNA stability of *FGF9* via the formation of a circITGB6/IGF2BP2/*FGF9* RNA–protein ternary complex.

FGF9 is required for circITGB6-induced CDDP resistance and M2 macrophage polarization

To further determine whether FGF9 is indispensable for circITGB6-mediated TAMs M2 polarization and subsequent induction of CDDP resistance, we added an FGF9-neutralizing antibody into coculture systems. Strikingly, the cell viability and colony formation of CDDP-treated cells were markedly inhibited by the FGF9-neutralizing antibody (online supplemental figure 14A-C). Moreover, CDDP-induced apoptosis and the number of γ-H2AX foci mediated by circITGB6 were drastically enhanced when FGF9 was blocked (online supplemental figure 14D-E). Supernatants harvested from OC cells (with vector-transfected or circITGB6-transfected) were used to treat the PBMC-derived $CD14^+$ monocytes. Blockade of FGF9 synergistically abolished the M2 macrophage polarization-promoting effect of FGF9, resulting in large numbers of M1 macrophages and few M2 macrophages (figure 6I–L). Additionally, the levels of the M2 markers CD206 and IL-10 were dramatically reduced, while those of the M1 markers CD80 and IL-6 were significantly increased in macrophages as measured by qRT-PCR (online supplemental figure 14F, G) and ELISA (online supplemental figure 14H, I) on FGF9 blockade.

Due to the current lack of FGF9-neutralizing antibody suitable for in vivo assays, we used CRISPR/Cas9-mediated gene knockout (KO) targeting FGF9 in ID8-circITGB6 cells for further in vivo assays. We first constructed FGF9-KO-ID8-circITGB6 cells (figure 6M). The results demonstrated that after FGF9 KO in ID8-circITGB6 cells, the effect of circITGB6 on CDDP resistance was significantly impaired (figure 6N,O) and survival was prolonged (figure 6P) compared with that of control cells in vivo. These findings suggested that circITGB6-mediated TAM M2 polarization and subsequent induction of CDDP resistance were dependent on FGF9 secretion in the TME of OC.

Targeting tumor-derived circITGB6 provides enhanced therapeutic benefits in OC

Given that circITGB6 promotes TAM M2 polarization, resulting in an immunosuppressive microenvironment and then conferring CDDP resistance, we reasoned that OC cell-derived circITGB6 may be a therapeutic target. Using antisense oligonucleotide (ASO) targeting, the circITGB6-specific back-splicing sequence, an in vivo optimized circITGB6 inhibitor, we successfully knocked down the expression of circITGB6, as confirmed by qRT-PCR (online supplemental figure 15A). As shown in figure 7A–D, compared with CDDP and phosphate buffer saline (PBS) administration group, CDDP and ASO-circITGB6 combination therapy dramatically suppressed tumor growth and increased the overall survival rate. In addition, significant decreases in the infiltrated $CD206^+$ M2 macrophages and FGF9 expression were found in the tumors of mice treated with the combination therapy (figure 7E–G). Moreover, the expression of the M2 markers IL-10 and Arg1 was significantly reduced in TAMs isolated from the tumors of mice administered ASO-circITGB6, while the expression of the M1 markers TNF-α and iNOS was markedly increased, as measured by ELISA (figure 7I,J) and qRT-PCR (figure 7K–M). In addition, FGF9 levels were markedly decreased in the tumor ascites of mice administered combination therapy, as detected by ELISA (online supplemental figure 15B). Moreover, we found that ASO-circITGB6 therapy dramatically decreased the $CD206^+$ M2 macrophage infiltration and increased the granzyme B^+ $CD8^+$ T-cell infiltration compared with PBS administration group (online supplemental figure 15D-F). Notably, we found that ASO-circITGB6 significantly increased the antitumor effect of PD-1 antibody in OC (online supplemental figure 16A-F).

Clinical relevance of the circITGB6/FGF9/M2 macrophage polarization axis in OC

IHC and ISH assays showed that the expression of *FGF9* and circITGB6 and the proportion of $CD206^+$ macrophages in chemoresistant OC tissues were markedly higher than those in chemosensitive OC tissues (figure 7N,O). Correlation analysis showed that high levels of circITGB6 were significantly associated with high *FGF9* expression and a high proportion of $CD206^+$ macrophages (figure 7O,P). Importantly, the correlation analysis showed that CDDP resistance was remarkably associated with high *FGF9* expression (online supplemental figure 15C). Moreover, the proportion of $CD206^+$ macrophages and the expression of *FGF9* were positively correlated in patients with OC (figure 7R). Additionally, Kaplan-Meier survival curves and log-rank tests revealed that patients with OC with combined high circITGB6 expression, high FGF9 expression, and a high proportion of infiltrated $CD206^+$ macrophages exhibited the shortest relapse-free survival (Figure 7S). Taken together, our findings suggest that circITGB6/IGF2BP2/*FGF9* forms an RNA–protein ternary complex to stabilize *FGF9*, inducing macrophage polarization toward an M2 phenotype and then leading to CDDP resistance, malignant progression, and poor clinical outcomes in human OC (figure 7T).

Figure 7

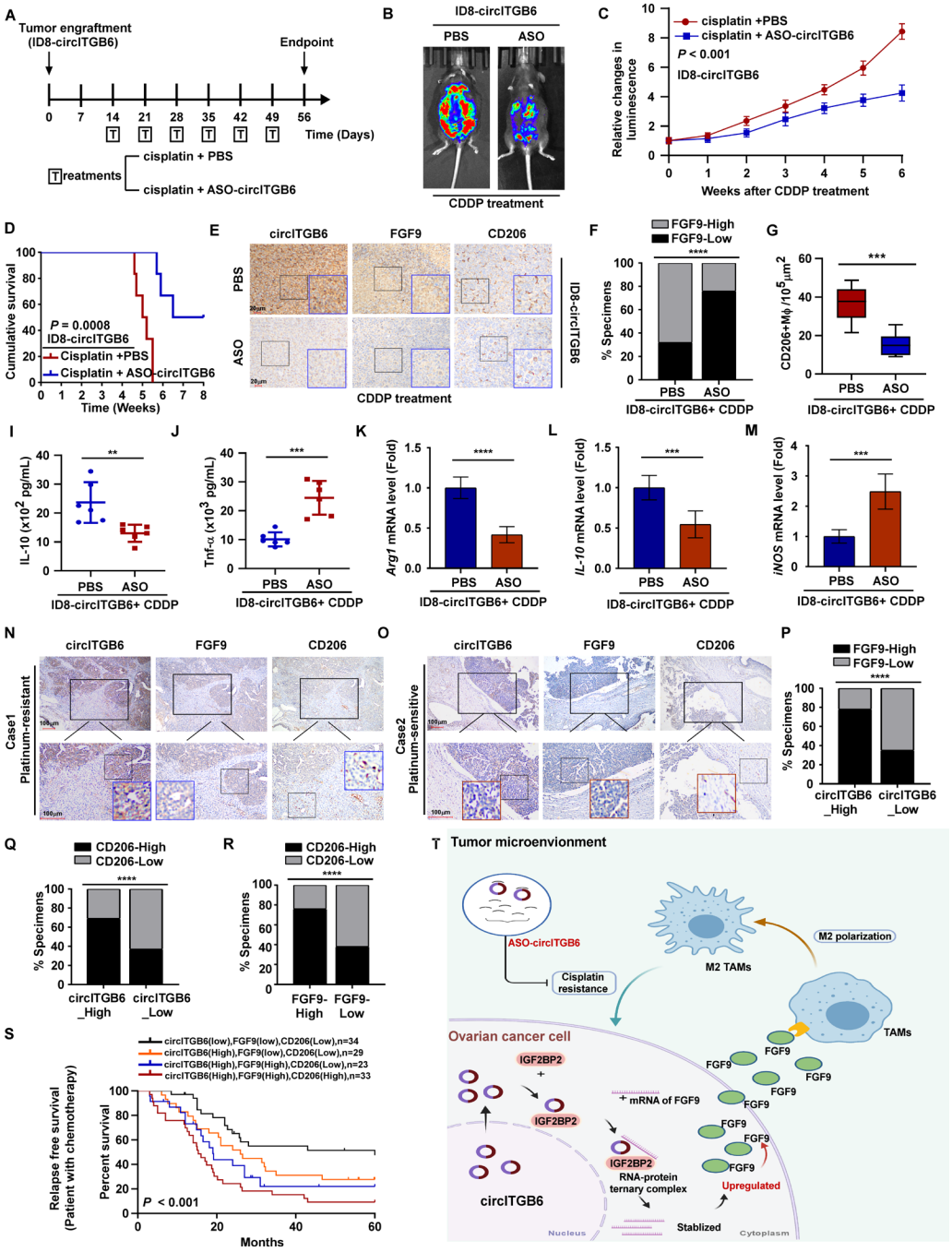

Figure 7 Clinical relevance of circITGB6/FGF9/M2 macrophages polarization in OC. (A) Schematic representation of xenograft tumor model. (B–D) Relative changes in bioluminescence signal and survival curve of intraperitoneal tumors in C57BL/6 mice in each group with different treatment. (E–G) circITGB6 ISH staining and FGF9 and CD206 immunohistochemistry staining of tumors treated with different therapies. Correlation analyses between FGF9 expression and different therapies in C57BL/6 mice tumor. The CD206$^+$ macrophage infiltration proportion from each group treated with different therapies were quantified. (I–M) Expression of IL-10, TNF-α, ARG1 and iNOS in the TAMs isolated from C57BL/6 mice tumor treated with different therapies measured by ELISA (I,J) and qRT–PCR (K–M). (N,O) Representative ISH staining for circITGB6 and IHC staining images of FGF9, CD206 in OC patient specimens (n=119). (P,Q) Correlation analysis showed that circITGB6 was significantly associated with FGF9 and CD206$^+$ macrophage infiltration proportion. χ^2 test was used. (R) Correlation analyses between FGF9 expression and CD206$^+$ macrophage infiltration proportion in OC patient specimen. (S) The patient specimens were divided into four groups according to circITGB6, FGF9, and CD206 expression. Kaplan-Meier survival curves showed that patients with OC with combined high circITGB6, FGF9 expression, and CD206 macrophage infiltration proportion significantly suffered the worst RFS. (T) A proposed model for the regulatory landscape of the circITGB6/IGF2BP2/*FGF9* signaling axis in promoting the CDDP resistance of OC. Results are presented as means±SD of a representative experiment performed in triplicate. *P<0.05, **P<0.01, ***P<0.001, ****P<0.0001. ASO, antisense oligonucleotide; CDDP, cisplatin; IL, interleukin; NS indicates no significance; OC, ovarian cancer; RFS, relapse-free survival; TAM, tumor-associated macrophage; TNF-α, tumor necrosis factor alpha.

DISCUSSION

Most patients with OC experience frequent recurrence, mainly due to the development of chemotherapy resistance.[29] Considerable efforts have been made to investigate the resistance mechanisms of cancer cells, including enhancement of CSCs, epigenetic alterations, decreased drug accumulation, and deregulation of apoptosis-related signaling.[30–32] Notably, with advances in NGS, coculture technologies, and novel analytic methods, the immune cells in the TME have been found to play a crucial role in the progression of multiple tumors. Emerging lines of evidence show that macrophages, the high infiltrated immune cells in the TME, contribute to chemoresistance.[33] However, the crosstalk between tumor cells and TAMs and its role in platinum resistance in OC remains largely unknown. In this study, we identified a novel circRNA, circITGB6, that modulates the TME and plays an important role in chemoresistance in OC. Importantly, circITGB6 enhanced the stability of *FGF9* mRNA by forming a circITGB6/IGF2BP2/*FGF9* ternary complex, which subsequently led to promotion of *FGF9*-mediated crosstalk between tumor cells and macrophages in the TME of OC, ultimately resulting in platinum resistance in patients with OC. These findings provide mechanistic and translational insight into the circRNA-mediated modulation of the TME that promotes platinum resistance in OC.

circRNAs are more stable than other non-coding RNAs, suggesting that they may have important functions. Importantly, emerging evidence has demonstrated that circRNAs serve as crucial regulators of immune cells, including macrophages, natural killer cells, and $CD8^+$ T cells in the TME.[21] In this study , we revealed that circITGB6 acts as a scaffold and facilitates the stabilizing effect of IGF2BP2 on mRNA of *FGF9*, thus leading to M2 polarization of TAMs. Although dysregulation of circRNAs in OC tissues has been previously reported, no prior study has explored the roles of circRNAs in regulating the crosstalk between cancer cells and macrophages in the TME of OC or investigated the feasibility of using circRNAs in serum as invasive biomarkers to predict the platinum therapy response status of patients with OC. Our data showed that circITGB6 expression was obviously increased in OC tissues and matched serum from patients with OC with chemoresistance resistance, and was accompanied by an increased number of infiltrated M2 macrophages.

circITGB6-induced *FGF9* was identified as the pivotal bridge of the cellular crosstalk between cancer cells and TAMs in this study. *FGF9* has been implicated as a regulator of the progression of several types of cancers and also participates in various pathological processes, including cancer growth and metastasis.[34–36] Importantly, recent studies have reported that *FGF9* can promote M2 macrophage polarization and alleviate adverse cardiac remodeling in the infarcted diabetic heart.[37] Additionally, *FGF9* has been reported to modulate macrophage M2 polarization and promote bladder cancer cell aggressiveness.[38] However, the underlying regulation mechanism of *FGF9* and M2 macrophage polarization in OC with CDDP resistance remains unclear. In this study, we found that circITGB6-overexpressing OC cell-derived *FGF9* indirectly affected the response to CDDP by inducing M2 macrophage polarization in an IGF2BP2/*FGF9* interaction-dependent manner. Thus, these findings uncover a novel mechanism for M2 macrophage polarization in OC and suggest that induction of *FGF9* mRNA degradation might be a promising strategy for platinum resistance blockade in OC.

The TME of OC is unique from that of other solid tumors because cancer cells easily dislodge from primary OC tissues into the peritoneal cavity and abdomen, where they produce a unique microenvironment containing immune cells, fibroblasts, adipocytes, and other lipid mediators.[6 7] TAMs, the major population of immune cells, exhibit important functions in tumor progression processes, including drug resistance.[39] DeNardo *et al* reported that M2-type macrophages foster paclitaxel resistance and metastasis via interaction with $CD8^+$ T cells in a paracrine manner in breast cancer.[40] It has also been reported that M2 macrophages can release some chemoprotective factors, including lysosomal enzymes and cathepsins B and S, thus protecting tumor cells from the direct cytotoxic efficacy.[41] Moreover, Jinushi *et al* showed that MFG-E8 released from M2-like macrophages induces classical CSC-related STAT3 signaling activation, which consequently enhances chemoresistance in colon cancer.[42] However, whether M2-like macrophages contribute to platinum resistance in OC remains unclear. Our study provides the first evidence that upregulation of circITGB6 plays an important role in mediating CDDP resistance via polarizing TAMs toward the M2 phenotype in an FGF9-dependent manner. Therefore, our study provides insights into the mechanism underlying TME-mediated CDDP resistance in OC.

Colony-stimulating factor 1 (CSF1)/colony stimulating factor 1 receptor (CSF1R) signaling is a key regulator of TAM differentiation, function, and survival and therefore may be regarded as an attractive target.[43–45] Consequently, there have recently been various clinical trials targeting the CSF1/CSF1R pathway; however, the clinical successes have been limited to only patients with diffuse-type giant cell tumors characterized by CSF1 gene chromosome one translocation.[46] Moreover, in preclinical models, neither small-molecule inhibitors nor antibodies targeting CSF1 have led to good therapeutic responses.[47] Furthermore, a confusing phenomenon has been observed: potent depletion of TAMs using the CSF1/CSF1R inhibitors in several xenograft models has failed to show antitumor effects. Kumar V *et al* suggested that inhibition of CSF1R reversed CSF1-induced limits on granulocyte recruitment and then fostered substantial accumulation of tumor-promoting polymorphonuclear MDSCs, contributing to tumor progression.[48]

Given that CSF1R inhibitors contribute to tumor progression, it is essential to discover a novel and effective target that regulates TAM M2 polarization. In this study, we administered an ASO targeting circITGB6 in

vivo and found that the ASO significantly suppressed M2 phenotype polarization and consequently enhanced sensitivity to CDDP treatment. Under this circumstance, rational combination with an ASO targeting circITGB6 may improve the curative effects of traditional platinum-based chemotherapy and reduce the side effects of CSF1/CSF1R inhibitors.

In summary, we have uncovered a novel cellular crosstalk clinical network involving the circITGB6/IGF2BP2/*FGF9* axis that can regulate macrophage M2-type polarization, OC CDDP resistance, and OC prognosis. Our study also provides a potential therapeutic strategy for targeting macrophages in the TME of OC. Rather than depleting macrophages by using CSF1/CSF1R inhibitors, as has been the aim of many therapies targeting macrophages thus far, re-educating these macrophages in the TME may have potent efficacy to not only abolish their protumor roles but also eventually enlist them to play an antitumor role. The combination of CDDP and an ASO targeting circITGB6 may create an opportunity for therapeutic intervention and further improve the prognosis of patients with OC with circITGB6 overexpression.

Author affiliations
[1]Collaborative Innovation Center for Cancer Medicine, State Key Laboratory of Oncology in South China, Sun Yat-sen University Cancer Center, Guangzhou, China
[2]Department of Gynecology, Guangdong Provincial People's Hospital, Guangdong Academy of Medical Sciences, Guangzhou, Guangdong, China
[3]Department of Biotherapy, Sun Yat-sen University Cancer Center, Guangzhou, Guangdong, China
[4]Joint Laboratory for Translational Cancer Research of Chinese Medicine of the Ministry of Education of the People's Republic of China, International Institute for Translational Chinese Medicine, Guangzhou University of Chinese Medicine, Guangzhou, China
[5]Department of Orthopaedic Surgery, Sun Yat-sen University First Affiliated Hospital, Guangzhou, Guangdong, China
[6]Department of Gynecology, Sun Yat-sen University First Affiliated Hospital, Guangzhou, Guangdong, China

Contributors HL, FL, XJ, and WZ carried out most of the experimental work; collected and analyzed the data; and conducted the western blot analysis, plasmid constructions, and RNA pull down assays. HL, FL, XJ, and TX conducted the RNA-seq, qRT-PCR, luciferase reporters, RIP, and FACS assays. QP, LC, JZ, DW, YL, MH, and YD collected tissues and patient information, and conducted IHC and survival analysis. HL, FS, CY , YH, JY, YT, and YH conducted animal studies. XJ, LC, HL, and FL conducted cell culture. HL, XJ, YT, and WZ performed the in vitro studies. YZ, LS, and J-CX raised the concept, design the experiments, wrote the manuscript, and supervised the project. All authors reviewed the manuscript. J-CX is responsible for the overall content as the guarantor.

Funding This study was funded by the National Key R&D Program of China (grant number 2018YFC1313400), the Guangdong Natural Science Foundation, Guangdong Province, China (grant number 2018A030310237), the National Natural Science Foundation of China (grant numbers 81773110, 81803079, 81902638, 81872118, 81901764), and the Science and Technology Planning Project of Guangdong Province, China (grant number 2017B020227003).

Competing interests There are no competing interests.

Patient consent for publication Not applicable.

Ethics approval This study involves human subjects and was approved by the institutional research ethics committee of Sun Yat-sen University Cancer Center (SL-B2021-396-01). Subjects gave informed consent to participate in the study before taking part.

Provenance and peer review Not commissioned; externally peer reviewed.

Data availability statement Data are available upon reasonable request.

ORCID iD
Jian-Chuan Xia http://orcid.org/0000-0002-1268-3967

REFERENCES

1 Siegel RL, Miller KD, Fuchs HE, *et al*. Cancer statistics, 2021. *CA A Cancer J. Clin.* 2021;71:7–33.
2 Bray F, Ferlay J, Soerjomataram I, *et al*. Global cancer statistics 2018: GLOBOCAN estimates of incidence and mortality worldwide for 36 cancers in 185 countries. *CA Cancer J Clin* 2018;68:394–424.
3 Tsibulak I, Zeimet AG, Marth C. Hopes and failures in front-line ovarian cancer therapy. *Crit Rev Oncol Hematol* 2019;143:14–19.
4 Davis A, Tinker AV, Friedlander M. "Platinum resistant" ovarian cancer: what is it, who to treat and how to measure benefit? *Gynecol Oncol* 2014;133:624–31.
5 Wang M, Zhao J, Zhang L, *et al*. Role of tumor microenvironment in tumorigenesis. *J Cancer* 2017;8:761–73.
6 Cai DL, Jin L-P. Immune cell population in ovarian tumor microenvironment. *J Cancer* 2017;8:2915–23.
7 Worzfeld T, Pogge von Strandmann E, Huber M, *et al*. The unique molecular and cellular microenvironment of ovarian cancer. *Front Oncol* 2017;7:24.
8 Pogge von Strandmann E, Reinartz S, Wager U, *et al*. Tumor-Host cell interactions in ovarian cancer: pathways to therapy failure. *Trends Cancer* 2017;3:137–48.
9 Asare-Werehene M, Communal L, Carmona E, *et al*. Plasma Gelsolin Inhibits $CD8^+$ T-cell Function and Regulates Glutathione Production to Confer Chemoresistance in Ovarian Cancer. *Cancer Res* 2020;80:3959–71.
10 Xue J, Schmidt SV, Sander J, *et al*. Transcriptome-Based network analysis reveals a spectrum model of human macrophage activation. *Immunity* 2014;40:274–88.
11 Lawrence T, Natoli G. Transcriptional regulation of macrophage polarization: enabling diversity with identity. *Nat Rev Immunol* 2011;11:750–61.
12 Reinartz S, Schumann T, Finkernagel F, *et al*. Mixed-polarization phenotype of ascites-associated macrophages in human ovarian carcinoma: correlation of CD163 expression, cytokine levels and early relapse. *Int J Cancer* 2014;134:32–42.
13 Dietze R, Hammoud MK, Gómez-Serrano M, *et al*. Phosphoproteomics identify arachidonic-acid-regulated signal transduction pathways modulating macrophage functions with implications for ovarian cancer. *Theranostics* 2021;11:1377–95.
14 Chen L-L, Yang L. Regulation of circRNA biogenesis. *RNA Biol* 2015;12:381–8.
15 Li Y, Zheng Q, Bao C, *et al*. Circular RNA is enriched and stable in exosomes: a promising biomarker for cancer diagnosis. *Cell Res* 2015;25:981–4.
16 Holdt LM, Stahringer A, Sass K, *et al*. Circular non-coding RNA ANRIL modulates ribosomal RNA maturation and atherosclerosis in humans. *Nat Commun* 2016;7:12429.
17 Geng Y, Jiang J, Wu C. Function and clinical significance of circRNAs in solid tumors. *J Hematol Oncol* 2018;11:98.
18 Zhao Z, Li X, Jian D, *et al*. Hsa_circ_0054633 in peripheral blood can be used as a diagnostic biomarker of pre-diabetes and type 2 diabetes mellitus. *Acta Diabetol* 2017;54:237–45.
19 Guarnerio J, Bezzi M, Jeong JC, *et al*. Oncogenic role of Fusion-circRNAs derived from cancer-associated chromosomal translocations. *Cell* 2016;165:289–302.
20 Su M, Xiao Y, Ma J, *et al*. Circular RNAs in cancer: emerging functions in hallmarks, stemness, resistance and roles as potential biomarkers. *Mol Cancer* 2019;18:90.

21 Zhang Q, Wang W, Zhou Q, *et al*. Roles of circRNAs in the tumour microenvironment. *Mol Cancer* 2020;19:14.
22 Pardoll DM. The blockade of immune checkpoints in cancer immunotherapy. *Nat Rev Cancer* 2012;12:252–64.
23 Aran D, Hu Z, Butte AJ. xCell: digitally portraying the tissue cellular heterogeneity landscape. *Genome Biol* 2017;18:220.
24 Song M, Yeku OO, Rafiq S, *et al*. Tumor derived UBR5 promotes ovarian cancer growth and metastasis through inducing immunosuppressive macrophages. *Nat Commun* 2020;11:6298.
25 Sánchez-González I, Bobien A, Molnar C, *et al*. miR-149 suppresses breast cancer metastasis by blocking paracrine interactions with macrophages. *Cancer Res* 2020;80:1330–41.
26 Holohan C, Van Schaeybroeck S, Longley DB, *et al*. Cancer drug resistance: an evolving paradigm. *Nat Rev Cancer* 2013;13:714–26.
27 Hafner M, Landthaler M, Burger L, *et al*. Transcriptome-Wide identification of RNA-binding protein and microRNA target sites by PAR-CLIP. *Cell* 2010;141:129–41.
28 Li J-H, Liu S, Zhou H, *et al*. starBase v2.0: decoding miRNA-ceRNA, miRNA-ncRNA and protein-RNA interaction networks from large-scale CLIP-Seq data. *Nucleic Acids Res* 2014;42:D92–7.
29 Vaughan S, Coward JI, Bast RC, *et al*. Rethinking ovarian cancer: recommendations for improving outcomes. *Nat Rev Cancer* 2011;11:719–25.
30 Chen S-H, Chang J-Y. New insights into mechanisms of cisplatin resistance: from tumor cell to microenvironment. *Int J Mol Sci* 2019;20. doi:10.3390/ijms20174136. [Epub ahead of print: 24 Aug 2019].
31 Gatti L, Zunino F. Overview of tumor cell chemoresistance mechanisms. *Methods Mol Med* 2005;111:127–48.
32 Norouzi-Barough L, Sarookhani MR, Sharifi M, *et al*. Molecular mechanisms of drug resistance in ovarian cancer. *J Cell Physiol* 2018;233:4546–62.
33 Correia AL, Bissell MJ. The tumor microenvironment is a dominant force in multidrug resistance. *Drug Resist Updat* 2012;15:39–49.
34 Hendrix ND, Wu R, Kuick R, *et al*. Fibroblast growth factor 9 has oncogenic activity and is a downstream target of Wnt signaling in ovarian endometrioid adenocarcinomas. *Cancer Res* 2006;66:1354–62.
35 Li ZG, Mathew P, Yang J, *et al*. Androgen receptor-negative human prostate cancer cells induce osteogenesis in mice through FGF9-mediated mechanisms. *J Clin Invest* 2008;118:2697–710.
36 Sun C, Fukui H, Hara K, *et al*. Fgf9 from cancer-associated fibroblasts is a possible mediator of invasion and anti-apoptosis of gastric cancer cells. *BMC Cancer* 2015;15:333.
37 Singla DK, Singla RD, Abdelli LS, *et al*. Fibroblast growth factor-9 enhances M2 macrophage differentiation and attenuates adverse cardiac remodeling in the infarcted diabetic heart. *PLoS One* 2015;10:e0120739.
38 Wu S, Xu R, Zhu X, *et al*. The long noncoding RNA LINC01140/miR-140-5p/FGF9 axis modulates bladder cancer cell aggressiveness and macrophage M2 polarization. *Aging* 2020;12:25845–64.
39 Colvin EK. Tumor-Associated macrophages contribute to tumor progression in ovarian cancer. *Front Oncol* 2014;4:137.
40 DeNardo DG, Brennan DJ, Rexhepaj E, *et al*. Leukocyte complexity predicts breast cancer survival and functionally regulates response to chemotherapy. *Cancer Discov* 2011;1:54–67.
41 Shree T, Olson OC, Elie BT, *et al*. Macrophages and cathepsin proteases blunt chemotherapeutic response in breast cancer. *Genes Dev* 2011;25:2465–79.
42 Jinushi M, Chiba S, Yoshiyama H, *et al*. Tumor-Associated macrophages regulate tumorigenicity and anticancer drug responses of cancer stem/initiating cells. *Proc Natl Acad Sci U S A* 2011;108:12425–30.
43 Lin EY, Nguyen AV, Russell RG, *et al*. Colony-Stimulating factor 1 promotes progression of mammary tumors to malignancy. *J Exp Med* 2001;193:727–40.
44 Hume DA, MacDonald KPA. Therapeutic applications of macrophage colony-stimulating factor-1 (CSF-1) and antagonists of CSF-1 receptor (CSF-1R) signaling. *Blood* 2012;119:1810–20.
45 Cannarile MA, Weisser M, Jacob W, *et al*. Colony-Stimulating factor 1 receptor (CSF1R) inhibitors in cancer therapy. *J Immunother Cancer* 2017;5:53.
46 Ries CH, Cannarile MA, Hoves S, *et al*. Targeting tumor-associated macrophages with anti-CSF-1R antibody reveals a strategy for cancer therapy. *Cancer Cell* 2014;25:846–59.
47 Conway JG, McDonald B, Parham J, *et al*. Inhibition of colony-stimulating-factor-1 signaling in vivo with the orally bioavailable cFMS kinase inhibitor GW2580. *Proc Natl Acad Sci U S A* 2005;102:16078–83.
48 Kumar V, Donthireddy L, Marvel D, *et al*. Cancer-Associated fibroblasts neutralize the anti-tumor effect of CSF1 receptor blockade by inducing PMN-MDSC infiltration of tumors. *Cancer Cell* 2017;32:654–68.